Computer Modeling in Engineering & Sciences
DOI:10.32604/cmes.2020.010565
Article

Milling Parameters Optimization of Al-Li Alloy Thin-Wall Workpieces Using Response Surface Methodology and Particle Swarm Optimization

Haitao Yue[1], Chenguang Guo[1,*], Qiang Li[1], Lijuan Zhao[1] and Guangbo Hao[2]

[1]School of Mechanical Engineering, Liaoning Technical University, Fuxin, 12300, China
[2]School of Engineering, University College Cork, Cork, T12 K8AF, Ireland
*Corresponding Author: Chenguang Guo. Email: gchg_neu@163.com
Received: 18 March 2020; Accepted: 16 June 2020

Abstract: To improve the milling surface quality of the Al-Li alloy thin-wall workpieces and reduce the cutting energy consumption. Experimental research on the milling processing of AA2195 Al-Li alloy thin-wall workpieces based on Response Surface Methodology was carried out. The single factor and interaction of milling parameters on surface roughness and specific cutting energy were analyzed, and the multi-objective optimization model was constructed. The Multi-objective Particle Swarm Optimization algorithm introducing the Chaos Local Search algorithm and the adaptive inertial weight was applied to determine the optimal combination of milling parameters. It was observed that surface roughness was mainly influenced by feed per tooth, and specific cutting energy was negatively correlated with feed per tooth, radial cutting depth and axial cutting depth, while cutting speed has a non-significant influence on specific cutting energy. The optimal combination of milling parameters with different priorities was obtained. The experimental results showed that the maximum relative error of measured and predicted values was 8.05%, and the model had high reliability, which ensured the low surface roughness and cutting energy consumption. It was of great guiding significance for the success of Al-Li alloy thin-wall milling with a high precision and energy efficiency.

Keywords: Al-Li alloy thin-wall workpieces; response surface methodology; surface roughness; specific cutting energy; multi-objective particle swarm optimization algorithm

1 Introduction

The Al-Li alloy, a lightweight with high-strength structural materials, is widely applied in aerospace industry in the 21st century via superior properties that provides low density, high specific strength, stiffness and excellent corrosion resistance [1,2]. The AA2195 Al-Li alloy belongs to the third-generation Al-Cu-Li alloy mainly used in space shuttle fuel tank, which is the most widely used material in the Weldalite series, and reduce the weight of 10% and increase the strength of 30% compared with the traditional Al alloy [3,4]. Scholars have shown great interest in the research and application development

of Al-Li alloy due to the excellent comprehensive properties, including mechanical properties [5], weldability [6,7], corrosion resistance [8,9] and other related research.

It is found that due to an improper selection of milling parameters for AA2195 Al-Li alloy often lead to less than 20% of the material utilization rate, the machine tools energy consumption is large, and the machining accuracy and surface roughness cannot meet the requirements. With a rapid development of aerospace industry, the demand for the lightweight, high-strength Al-Li alloy is also increasing. Therefore, how to select milling parameters reasonably to improve the surface roughness of AA2195 Al-Li alloy thin-wall workpieces and reduce the machine tools energy consumption becomes particularly crucial.

Over the past decade, extensive researches were conducted to improve surface roughness and reduce energy consumption of Al-based materials by using different approaches. For instance, Mou et al. [10] analyzed the influence of milling parameters on the Al-Li alloy surface roughness through orthogonal experiment, which supplied the experimental basis for the improvement of the fatigue properties of Al-Li alloy by using the mechanical milling process. Sahoo et al. [11] proposed an optimization method combining weighted principal component analysis with Response Surface Methodology (RSM) to achieve good surface finish and lower tool vibration in CNC turning process of 63400 Al alloy. Yahya et al. [12] adopted the RSM to establish the relationship model of AA6061 surface roughness with machining parameters, and determined the significance of each parameter. They confirmed RMS was an efficient and robust technique from the observations of optimization error. Hussain et al. [13] adopted grey correlation analysis and Taguchi method to conduct surface roughness optimization research investigation on the milling parameters of 6063 Al alloy, and the results showed that the proposed method was feasible and applicable for continuous improvement in product quality in manufacturing industry. Liu et al. [14] presented a novel model for predicting surface roughness when slot milling Al-7075 and validated the proposed model by experiments under various cutting conditions. The model was straightforward, thus providing great potential for surface roughness control in real production. In order to reduce the energy consumption, Zhang et al. [15] optimized the process parameters by the model with the specific cutting energy consumption and the processing time, provided an efficient solution to reduce the impact of the environment caused by energy consumption and to realize the sustainable manufacturing. Carmita [16] employed the RSM to generate the regression model for the electrical energy consumed and surface roughness during slot milling of AISI 6061 T6 and reduced the environmental impacts on the related to the milling process without compromising the performance and quality of the final product.

Besides lots of experiments and complicated mathematical models, the optimization of process parameters can be achieved by the implementation of advanced optimization tools such as Particle Swarm Optimization (PSO), Multi-objective PSO (MOPSO), hybrid PSO. Rashmi et al. [17,18] studied the parameters influence on milling force, surface roughness and energy consumption in AA6061 Al material milling systematically, and determined the optimal parameters by PSO. Here, the authors found that the PSO successfully optimized the process parameters. Singh et al. [19] adopted two evolutionary optimization methods, namely PSO and bacteria foraging optimization (BFO), for the optimization of maximum tool flank wear. They found the PSO outperformed BFO in terms of time saving and better convergence due to lesser number of steps. Gupta et al. [20] introduced the PSO along with the teaching learning-based optimization approach to optimize process parameters. Here, both algorithms proved to be highly effective, with the PSO being concluded as the best amongst the two. Li et al. [21] developed the regression models based on the experimental data, and the optimal parameters for minimizing energy and time were determined through the MOPSO algorithm. The authors drawn a trade-off point successfully between the low processing time and high energy efficiency. Jang et al. [22] used the artificial neural networks PSO (ANN-PSO) to find cutting conditions to minimize the specific cutting energy in a milling

process. The results shown that the overall error between the model prediction and experiment at the optimized cutting conditions obtained from the ANN-PSO was less than 1%. Zhou et al. [23] proposed an integrated optimization method with grey relational analysis (GRA), radial basis function (RBF) neural network and PSO to simultaneously obtain minimum surface roughness and maximum compressive residual stress. Verification experiments shown that a higher improvement was obtained with the proposed method (62.87%) than that of the original GRA (50.00%).

The above scholars have an important guiding significance for the improvement of the surface roughness and reduce energy consumption of Al-based lightweight and high-strength materials. Meanwhile, the PSO methods prove a great success when it is required to tackle complex engineering application derived from experiments. However, there are relatively few reports on the study of surface roughness and energy consumption when end milling of Al-Li alloy thin-wall workpieces, especially on the optimization of machining parameters.

Therefore, this work explored the feasibility for multi-objective optimization with the RSM-PSO method. The Central Composite Design (CCD) was applied to experimentally establish data of AA2195 Al-Li alloy thin-wall workpieces to study the effect of process parameters (cutting speed (v), feed per tooth (f_z), radial cutting depth (a_e) and axial cutting depth (a_p)) on the responses such as surface roughness (R_a) and specific cutting energy (e_s). By adopting the ANOVA and RSM, the interaction between the process parameters were analyzed and the response models were acquired. The Adaptive Chaos Multi-objective Particle Swarm Optimization (AC-MOPSO) algorithm was used to determine the optimal parameters combination with different priorities, and the results were verified through confirmation experiments.

2 Milling Experiments of AA2195 Al-Li Alloy

2.1 Experimental Materials and Equipment

The 4 mm diameter with tungsten steel matrix and PVD-TiAlN coating cutting tool cutter is adopted to carry out dry milling on the XK540F milling machine for the 2195 Al-Li alloy thin-wall workpieces after T6 artificial aging treatment, as shown in Fig. 1. The size of workpieces is 110 mm × 80 mm × 8 mm, and its chemical composition is shown in Tab. 1. The Kistler mutli-component dynamometer is adopted to measure the milling force along the X, Y and Z directions. Upon using the Roughness detector and KEYENCE VHX-5000 optical ultra-depth microscope to observe the surface roughness and macroscopic morphology of the workpieces, respectively.

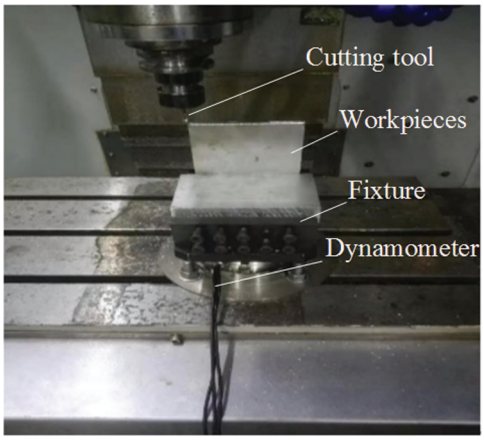

Figure 1: The milling experiment

Table 1: Chemical composition of 2195 Al-Li alloy (ω/%)

Cu	Li	Mg	Ag	Zr	Ti	Al
3.7~4.3	0.8~1.2	0.25~0.8	0.25~0.6	0.08~0.16	0.1	Bal.

2.2 Experimental Design

The RSM is a comprehensive optimization method for experimental design and modeling. Upon combining experimental methods, the RSM could obtain accurate correlation between target and factors with fewer experiments and higher modeling accuracy. The CCD is adopted to establish the central composite matrix with 6 replicated center points and 24 axial points for four factors and two levels, namely, 6 groups of central experiments, 24 groups of factorial experiments, a total of 30 groups of central composite design experimental schemes. Each factor is defined as 5 levels: ±α (axial point, α = 2), ±1 (factorial point) and 0 (center point), as shown in Tab. 2.

Table 2: Ranges and designations of the studied process factors

Level	Cutting speed (m/min)	Feed per tooth (mm/z)	Radial cutting depth (mm)	Axial cutting depth (mm)
+α	80	0.1	2.8	1.2
1	65	0.08	2.6	1.0
0	50	0.06	2.4	0.8
−1	35	0.04	2.2	0.6
−α	20	0.02	2.0	0.4

2.3 Specific Cutting Energy

The specific cutting energy is defined as the energy required to remove a specific volume of workpiece material [24,25]. A smaller specific cutting energy, and a higher the energy efficiency. In this study, the model is established based on the effective cutting energy, which only considered the energy consumption of the milling area in the material removal process [22,26]. The model was shown in Eq. (1):

$$e_s = \frac{P_M}{MRR} \tag{1}$$

where P_M denotes the milling power (W) and MRR is the volumetric material removal rate (mm^3/s).

$$P_M = F_M \times v \tag{2}$$

where F_M is the milling resultant force (N) obtained by Eq. (3):

$$F_M = \sqrt{F_X^2 + F_Y^2 + F_Z^2} \tag{3}$$

The volumetric material removal rate MRR [26,27] is shown in Eq. (4):

$$MRR = a_e \times a_p \times f_z \times z \times n \tag{4}$$

where a_e is the radial milling depth (mm), z is the number of milling cutter edges, $z = 2$, and n denotes the spindle speed.

2.4 Multi-Objective Optimization Method

To solve the multivariable and nonlinear optimization problem with constraints, an effective algorithm is necessary. The PSO [28,29] is a stochastic computation algorithm proposed by Kennedy and Eberhart in 1995. PSO is widely applied in industrial optimization for its simple arithmetic, good robustness and high dependability. In this paper, we propose a modified MOPSO to analyze the trade-off between multiple objective functions.

2.4.1 PSO Algorithm

The PSO algorithm randomly initializes swarm $X = (x_1, x_2, \cdots, x_N)$; in the feasible solution D-dimensional space. The all particles is N, the position, the velocity and the optimal position of particle i are expressed as $x = \left(x_i^1, x_i^2, \cdots, x_i^D\right)$, $v = \left(v_i^1, v_i^2, \cdots, v_i^D\right)$ and $pBest_i = \left(p_i^1, p_i^2, \cdots, p_i^D\right)$, respectively, and the global optimal position is expressed as $gBest = \left(p_g^1, p_g^2, \cdots, p_g^D\right)$. For the k^{th} iteration, the position and the velocity of the D-dimension particle i are updated by Eqs. (5) and (6):

$$v_i^d = \omega v_i^d + c_1 r_1 \left(p_i^d - x_i^d\right) + c_2 r_2 \left(p_g^d - x_i^d\right) \tag{5}$$

$$x_i^d = x_i^d + v_i^d \tag{6}$$

where, $1 \le i \le N$, ω is the inertial weight factor; c_1 and c_2 are the acceleration coefficients; r_1 and r_2 are the random numbers obey U (0, 1); p_i^d and p_g^d are the individual optimal position of the i^{th} particle and the d^{th} component of the global optimal position; v_i^d is the d^{th} component of the i^{th} generation particle velocity v_i; $v_i^d \in [v_{min,d}, v_{max,d}]$, taking the boundary value when the particle updating exceeds the boundary.

2.4.2 AC-MOPSO Algorithm

The MOPSO algorithm [21,23] is established on the basis of PSO algorithm, which has the advantages of diverse non-inferior solutions, rapid computational efficiency and solution speed, and has become an effective means to solve multi-objective optimization problems. The MOPSO algorithm is composed of external archive maintenance and global optimal position selection and update, which solves the dominant situation between individuals based on the Pareto relationship, and selects the individual and the global optimal position according to the external archive information and crowded distance. In this paper, the Chaos Local Search (CLS) algorithm and the adaptive inertial weight are introduced in MOPSO algorithm. The best 20% particles which remains for the sorting of fitness function values are performed by the CLS algorithm. Upon shrinking the search area and randomly generated the remaining 80% particles, which can prevent the particles falling into the local optimal solution. After updating the position and the velocity, the inertial weight is updated via Eq. (7) for balancing the local search and improvement, and speeding up the convergence of the algorithm.

$$\omega = \begin{cases} \omega_{\min} - \dfrac{(\omega_{\max} - \omega_{\min})\left(p_i^d - p_{\min}^d\right)}{\left(p_{avg}^d - p_{\min}^d\right)} \\ \omega_{\max} \end{cases} \tag{7}$$

where, ω_{min}, ω_{max} are the minimum and maximum inertial weight; p_{avg}^d and p_{min}^d are the mean and minimum values of all the particles before the iteration.

The step flowchart is shown in Fig. 2, and the steps are as follows:

Step 1: Initializing the x_i^k and v_i^k randomly, where $1 \le i \le N$. The particle swarm size is N, the inertial weight is ω, the acceleration coefficient are c_1 and c_2, the particle velocity boundary is $[v_{min,d}, v_{max,d}]$. Evaluating the initial particle fitness function value $P(\zeta)$.

Step 2: Creating and initializing the external archive matrix A_k.

Step 3: Evaluating the each particle fitness function value $p(\zeta)_i^k$ based on the dominance relationship between the objectives, obtaining the $pBest_i^k$ and $gBest^k$, storing the each particle x_i^k and $p(\zeta)_i^k$ in $pBest_i^k$, and the position and fitness value of the optimal individual in $pBest_i^k$ are stored in A_k.

Step 4: Calculating the crowded distance for all $pBest_i^k$ in A_k and sorted them, and remaining the best 20%. Performing the CLS algorithm and updating the $pBest_i^k$ and $gBest^{k+1}$.

Step 5: Satisfying the termination condition, ending and outputting the Pareto front solutions $gBest^{k+1}$. Otherwise, performing the **Step 6**.

Step 6: Updating the velocity v_i^{k+1}, the position x_i^{k+1} and the inertial weight ω.

Step 7: Maintaining the external archive matrix according to the crowded distance, forming A_{k+1} and performing the **Step 3**.

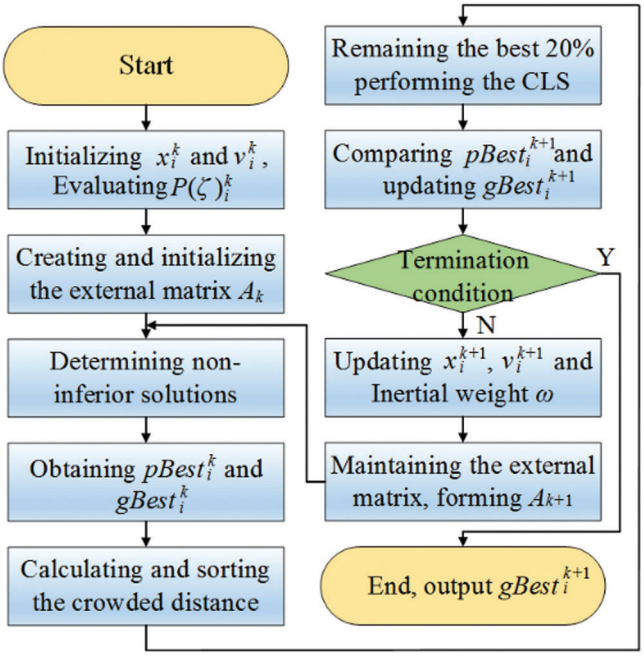

Figure 2: The AC-MOPSO algorithm flowchart

3 Results and Discussion

3.1 Establishment of Regression Model

The experimental design and results are shown in Tab. 3. The significance of regression model, model coefficient, and the lack of fit are carried out, and the optimal fitting model is selected according to the fitting analysis results. The step-wise regression method is used to eliminate the non-significant model terms, and the statistics R^2, adjusted R^2, precision R^2 and Adeq precision are calculated to confirm the accuracy of the response models. To verity the models adaptability and the correlation between the model predicted values

Table 3: The experimental design and results

Std. order	Run order	Factors				Response values	
		v (mm/s)	f_z (mm/z)	a_e (mm)	a_p (mm)	Ra (μm)	e_s (J/mm^3)
11	1	35	0.08	2.2	1	0.7403	4.6839
6	2	65	0.04	2.6	0.6	0.4529	12.8984
3	3	35	0.08	2.2	0.6	0.6974	7.4802
18	4	80	0.06	2.4	0.8	0.6453	7.5867
26	5	50	0.06	2.4	0.8	0.6397	6.7325
16	6	65	0.08	2.6	1	0.8081	4.9808
13	7	35	0.04	2.6	1	0.4813	9.7369
14	8	65	0.04	2.6	1	0.4767	9.2989
29	9	50	0.06	2.4	0.8	0.6503	6.7505
20	10	50	0.1	2.4	0.8	0.8791	4.8451
24	11	50	0.06	2.4	1.2	0.6628	5.4264
5	12	35	0.04	2.6	0.6	0.4553	14.5093
22	13	50	0.06	2.8	0.8	0.6387	6.5174
30	14	50	0.06	2.4	0.8	0.6309	6.4718
10	15	65	0.04	2.2	1	0.5023	10.7262
8	16	65	0.08	2.6	0.6	0.7279	6.5246
17	17	20	0.06	2.4	0.8	0.5965	8.0892
21	18	50	0.06	2	0.8	0.6683	8.7903
15	19	35	0.08	2.6	1	0.7350	4.5199
19	20	50	0.02	2.4	0.8	0.3461	17.4914
9	21	35	0.04	2.2	1	0.4880	10.9840
2	22	65	0.04	2.2	0.6	0.5186	15.4339
27	23	50	0.06	2.4	0.8	0.6557	6.9112
7	24	35	0.08	2.6	0.6	0.7410	6.9184
12	25	65	0.08	2.2	1	0.7693	5.1675
23	26	50	0.06	2.4	0.4	0.6223	11.9397
4	27	65	0.08	2.2	0.6	0.7524	7.8169
25	28	50	0.06	2.4	0.8	0.6414	6.5416
1	29	35	0.04	2.2	0.6	0.4691	16.0254
28	30	50	0.06	2.4	0.8	0.6039	6.7303

and the experimental results, the normal distribution probability of residuals are analyzed and the predicted values are compared with the experimental values, as shown in Figs. 3 and 4, respectively. Fig. 3 indicates the residuals of each response model are normally distributed on a straight line, showing that the residuals are evenly distributed and the model had adaptability. As shown in Fig. 4, each response model have a high prediction accuracy.

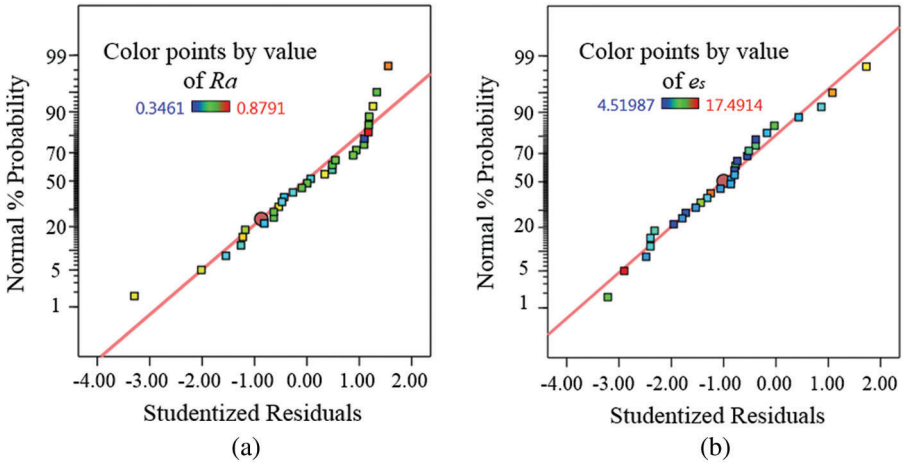

Figure 3: The normal distribution probability (a) surface roughness (b) specific cutting energy

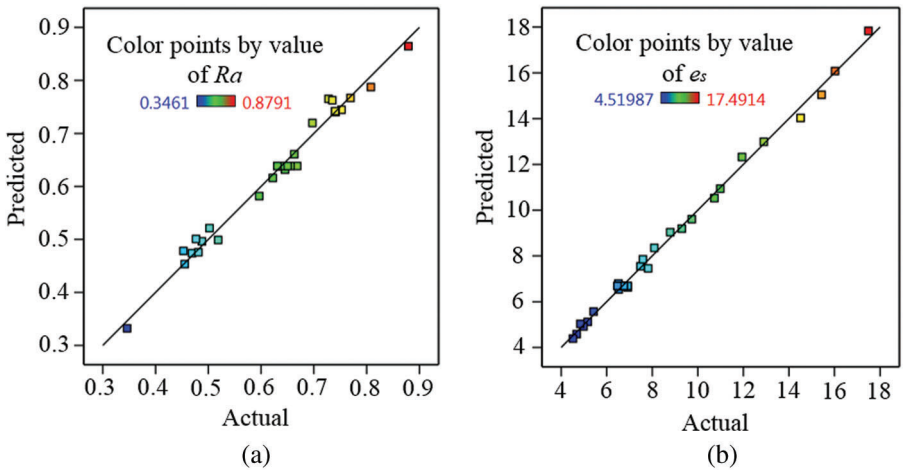

Figure 4: The comparison diagram between the models predicted and experimental values (a) surface roughness (b) specific cutting energy

3.2 Regression Model and ANOVA of Surface Roughness

The ANOVA results of surface roughness is shown in Tab. 4, and the F-value of 58.55 implies the model is significant. The R^2 of 0.9035 indicates a high correlation between the predicted values and experimental results. The adjusted R^2 and predicted R^2 approaches 1, and the difference between adjusted R^2 and predicted R^2 is less than 0.2, while Adeq precision is greater than 4, which verifies the model reliability. The p-value < 0.05 indicates that the model term is significant. For the surface roughness model, the f_z is the significant model term, as shown in Eq. (8):

$$Ra = 0.2028 + 0.0008v + 6.6525f_z - 0.0247a_e + 0.0557a_p \tag{8}$$

Fig. 5a shows the perturbation diagram of the influence of each milling parameter on the surface roughness. Fig. 5b demonstrates that the surface roughness is increased with the elevated feed per tooth and cutting speed. At 0.04 z/mm feed per tooth and 20 m/min cutting speed, the minimum value of surface roughness is achieved. The reason for the worse surface roughness with elevated feed per tooth is speculated that the workpiece material near the center line during the milling machining removes by

Table 4: The ANOVA for surface roughness

Source	Sum of square	df	Mean square	*F*-value	*p*-value prob > F	
Model	0.4321	4	0.1080	58.55	<0.0001	Significant
v	0.0037	1	0.0037	2.01	0.1685	
f_z	0.4249	1	0.4249	230.24	<0.0001	
a_e	0.0006	1	0.0006	0.3165	0.5787	
a_p	0.0030	1	0.0030	1.61	0.2155	
Residual	0.0461	25	0.0018			
Lack of fit	0.0199	20	0.0010	0.1896		Not significant
Pure error	0.0262	5	0.0052			
Cor total	0.4783	29				
Std. Dev.	0.0430		R^2	0.9035		
Mean	0.6288		Adjusted R^2	0.8881		
C.V.%	6.83		Predicted R^2	0.8844		
PRESS	0.0553		Adeq Precision	30.3476		

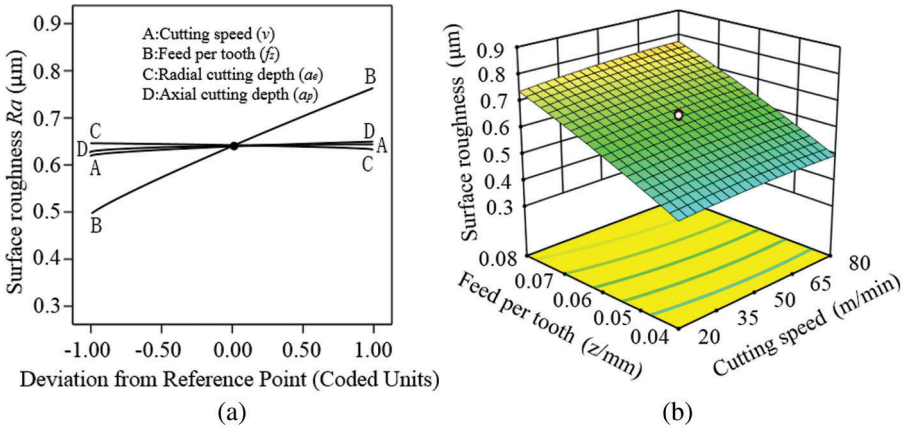

Figure 5: (a) Perturbation plot showing the effects of parameters on surface roughness. (b) Interaction effect of feed per tooth and cutting speed on surface roughness

shearing action, and the materials will not be completely crushed and residue in the bottom of the groove with the elevated feed of tooth. The defects (such as the pits, micro-cracks and matrix material tearing) are obviously increased, and the surface roughness is increased due to a decrease in surface quality. The surface roughness is slightly increased with the elevated cutting speed and axial cutting depth, and this finding is similar to the outcomes of Sen et al. [30]. It is possible that a higher cutting speed lead to the cutter eccentricity increases, and the impact between the tool and the workpiece material increases resulting in lots of scratches. Moreover, the milling force, friction and tool deformation increase with the elevated depth of cut, which resulting in the deposition of material on the rake face of the cutting tool and phenomenon helps to increase the surface roughness. Radial cutting depth has non-significant effect on the surface roughness.

3.3 Regression Model and ANOVA of Specific Cutting Energy

The ANOVA results of specific cutting energy are shown in Tab. 5, the F-value of 113.08 indicates the model is extremely significant. The lack of fit is not significant, implying that the model is reliable. The R^2 of 0.9906 and the Adeq Precision of 38.5314 indicates that the experimental values has a high correlation with the predicted values and the model has a strong recognition ability, respectively. For the model of e_s, the significant model terms are f_z, a_e and a_p, interaction terms $f_z a_p$, quadratic terms v^2, f_z^2, a_e^2 and a_p^2. The model of e_s is shown in the Eq. (9):

$$\begin{aligned} e_s = {} & 135.8295 - 0.1892v - 855.7500f_z - 54.2133a_e - 55.5392a_p + 0.7887vf_z - 0.0407va_e \\ & + 0.0523va_p + 70.6438f_z a_e + 136.4531f_z a_p + 4.5001a_e a_p + 0.0019v^2 + 3146.5104f_z^2 \\ & + 9.5001a_e^2 + 15.9326a_p^2 \end{aligned} \tag{9}$$

Table 5: The ANOVA for specific cutting energy

Source	Sum of square	df	Mean square	F-value	p-value prob > F	
Model	381.10	14	27.22	113.08	<0.0001	Significant
v	0.3790	1	0.3790	1.57	0.288	
f_z	245.84	1	245.85	1021.22	<0.0001	
a_e	7.57	1	7.57	31.43	<0.0001	
a_p	68.46	1	68.46	284.39	<0.0001	
vf_z	0.8957	1	0.8957	3.72	0.0729	
va_e	0.2383	1	0.2384	0.9900	0.3355	
va_p	0.3932	1	0.3932	1.63	0.2207	
$f_z a_e$	1.28	1	1.28	5.31	0.0360	
$f_z a_p$	4.77	1	4.77	19.80	0.0005	
$a_e a_p$	0.5186	1	0.5186	2.15	0.1628	
v^2	4.98	1	4.98	20.68	0.0004	
f_z^2	43.45	1	43.45	180.48	<0.0001	
a_e^2	3.96	1	3.96	16.45	0.0010	
a_p^2	11.14	1	11.14	46.28	<0.0001	
Residual	3.61	15	0.2407			
Lack of fit	1.08	10	0.1078	0.2129	0.9818	Not significant
Pure error	2.53	5	0.5065			
Cor total	384.71					
Std. Dev.	0.4906		R^2	0.9906		
Mean	8.56		Adjusted R^2	0.9819		
C.V.%	5.73		Predicted R^2	0.9744		
PRESS	9.86		Adeq Precision	38.5314		

The perturbation plot shows that the effects of the parameters on specific cutting energy in Fig. 6a. Fig. 6b shows the specific cutting energy decreases significantly with increasing feed per tooth and radial cutting depth. At 0.08 z/mm feed per tooth and 2.6 mm radial cutting depth, the minimum value of

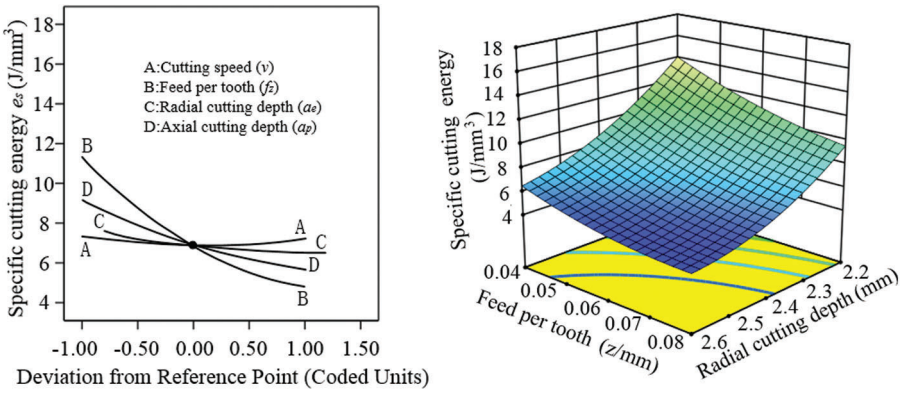

(a) (b)

Figure 6: (a) Perturbation plot showing the effects of parameters on specific cutting energy. (b) Interaction effect of feed per tooth and radial cutting depth on specific cutting energy

specific cutting energy is acquired. The feed per tooth, radial cutting depth and axial cutting depth have obvious negative influence on specific cutting energy, and the normal stress on the rake face of the cutting tool increases via their increasing, while the friction factor and stress decreases. Meanwhile, the decreasing friction angle causes the elevated shear angle and the decreasing deformation of the material, so that a low specific cutting energy. The cutting speed has non-significant influence on specific cutting energy, because the cutting speed is only related to the energy consumption of plastic deformation of material, while the effect of specific cutting energy and friction energy consumption is not [31]. The finding is consistent to the result of the work published by Carmita [16]. Nonetheless, an elevated cutting speed increases the heat in the cutting zone and helps to soften the material [30]. It decreases the strength and hardness of the processed metal. This is beneficial for reducing spindle energy consumption and tool wear.

4 Multi-Objective Optimization Model

4.1 Objective Function

In this paper, the surface roughness and specific cutting energy of AA2195 Al-Li alloy thin-wall workpieces milling are optimized. The optimization objective functions are shown in Eqs. (8) and (9).

4.2 Constraints

To determine the optimal parameters combination of AA2195 Al-Li alloy thin-wall workpieces milling, the constraints of cutting speed, feed per tooth, radial cutting depth, axial cutting depth, machine spindle power, spindle torque and surface roughness should be satisfied. The specific constraints are shown in followings:

1. The cutting speed: $v_{min} \le v \le v_{max}$, where v_{min} and v_{max} are set the minimum and maximum n of the machine tool respectively.
2. The feed per tooth: $f_{z\ min} \le f_z \le f_{z\ max}$, where $f_{z\ min}$ and $f_{z\ max}$ are the minimum and maximum f_z when milling processing.
3. The radial cutting depth: $a_{e\ min} \le a_e \le a_{e\ max}$, where $a_{e\ min}$ and $a_{e\ max}$ are the minimum and maximum a_e allowed for milling processing.
4. The axial cutting depth: $a_{p\ min} \le a_p \le a_{p\ max}$, where $a_{p\ min}$ and $a_{p\ max}$ are the minimum and maximum a_p allowed for milling processing.
5. Machine spindle power constraints: $P_c \le \eta P_{max}$, where η is the machine tool efficiency and P_{max} is the machine tool rating.

6. Spindle torque constraint: $F_cD/(2 \times 10^3) \leq T_{max}$, where F_c is the circumferential force of cutter milling, D is the cutter diameter, and T_{max} is the maximum allowable spindle torque of machine tool.
7. Surface roughness constraint: $Ra = 318f_z/[\tan(L_a) + \cot(C_a)] \leq Ra_{\max}$, where, L_a and C_a is the rake angle and the relief angle of the milling cutter respectively, and $Ra_{\max}$ is the maximum allowable surface roughness.

In conclusion, the multi-objective optimization model of Al-Li alloy thin-wall milling parameters can be expressed as:

$$\text{Min}[F(x)] = \text{Min}\left[Ra\left(n, f_z, a_e, a_p\right), e_s\left(n, f_z, a_e, a_p\right)\right] \tag{10}$$

$$S.t.\begin{cases} n_{\min} \leq n \leq n_{\max} \\ f_{z\min} \leq f_z \leq f_{z\max} \\ a_{e\min} \leq a_e \leq a_{e\max} \\ a_{p\min} \leq a_p \leq a_{p\max} \\ P_c \leq \eta P_{\max} \\ F_cD/(2 \times 10^3) \leq T_{\max} \\ 318f_z/[\tan(L_a) + \cot(C_a)] \leq Ra_{\max} \end{cases}$$

4.3 AC-MOPSO Algorithm Optimization Results

The AC-MOPSO algorithm is adopted to optimize the multi-objective optimization model. The algorithm population size is $N = 100$, the number of iterations is 2000, the inertia weight is $\omega_{max} = 0.9$, $\omega_{min} = 0.6$, the independent variable search area ranges from [−10, 10], the CLS algorithm maximum step is 10, and the learning factor $c_1 = c_2 = 2$. Three representative parameter combinations are selected from the non-inferior solutions, which are the optimal Ra, the optimal e_s and the two objectives with the same priority. The optimization results are shown in Fig. 7 and Tab. 6.

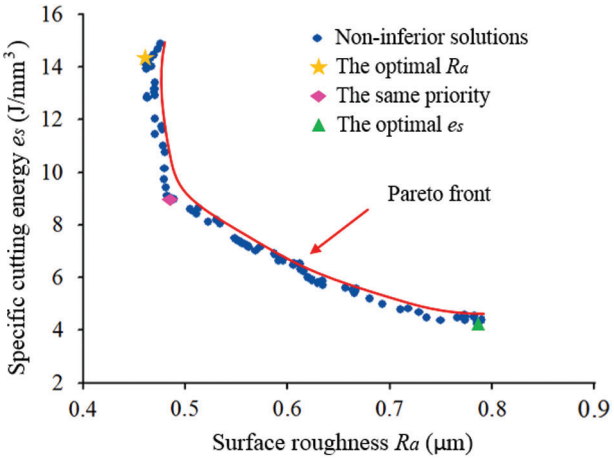

Figure 7: The AC-MOPSO algorithm solutions for optimization

The verification experiments are carried out on the same CNC milling machine, and the comparison results are shown in Tab. 7. The results shown that the maximum relative error between the experimental results and the predicted values of surface roughness and specific cutting energy is 8.05%, and the surface quality is good when the machined surface was is observed with the optical microscope at magnification of 200, as shown in Fig. 8.

Table 6: The optimal parameter combinations and results

No.	Factors				Response values	
	v (m/min)	f_z (mm/z)	a_e (mm)	a_p (mm)	Ra (μm)	e_s (J/mm^3)
1	35	0.04	2.6	0.4	0.461	14.152
2	65	0.04	2.6	0.8	0.482	9.074
3	55	0.08	2.5	0.8	0.786	4.220

Table 7: The verification experiment results

No.	Ra			e_s		
	Experimental	Predicted	Relative error	Experimental	Predicted	Relative error
1	0.461	0.454	1.54	14.152	15.077	6.14
2	0.482	0.494	2.43	9.074	9.868	8.05
3	0.786	0.802	1.99	4.220	4.411	4.33

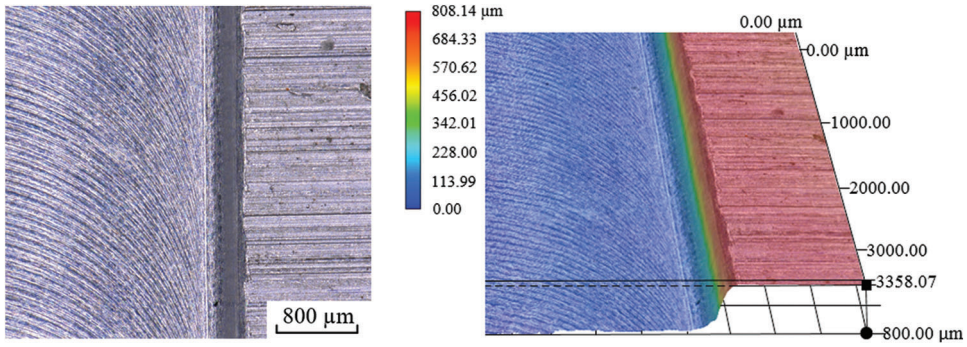

(a) (b)

Figure 8: The verification experiment observations (a) The machined surface (b) The three-dimensional shape

5 Conclusion

In this paper, the CCD was adopted to design the AA2195 Al-Li alloy thin-wall workpieces milling experiment scheme. The influence of milling parameters such as the cutting speed, feed per tooth, radial cutting depth and axial cutting depth on the surface roughness and specific cutting energy were studied by ANOVA and RSM, and the prediction models were established. The multi-objective optimization model was solved that go through the AC-MOPSO algorithm, so as that to determine the optimal milling parameter combination, and the accuracy of the prediction model was verified by experiments. The results were shown in followings:

1. The correlation analysis of machining performances signified that the improvement of surface roughness was achieved once a decrease in the feed per tooth, cutting speed and axial cutting depth. Conversely, the increasing in feed per tooth, radial cutting depth and axial cutting depth produced a low specific cutting energy.

2. The ranges of statistical parameters such as the statistics R^2, adjusted R^2, precision R^2 and adeq precision revealed that the RSM effectively developed a relationship between input and machining responses.
3. The AC-MOPSO algorithm introduced the chaos local search and the adaptive inertial weight was applied to obtain the non-inferior solutions of the multi-objective optimization model, and the optimal parameter combinations with different priorities were obtained, respectively.
4. The v of 35 m/min, f_z of 0.04 z/mm, a_e of 2.6 mm and a_p of 0.4 mm are the best parameter combination for minimizing R_a (0.461 μm). When the v and a_p are increased to 65 m/min and 0.8 mm respectively, the equal priority of R_a and e_s are acquired. The best solution corresponds v of 55 m/min, f_z of 0.08 z/mm, a_e of 2.5 mm and a_p of 0.8 mm, which gives minimum e_s (4.220 J/mm^3).
5. The verification experiments shown that the maximum relative error between the experimental results and model predicted values of surface roughness and specific cutting energy was 8.05%. The experiment results demonstrated the validity for the models. The expectation of lower surface roughness and cutting energy consumption was realized.

In future, the optimal parameters of Al-Li alloy can be studied in milling or other conventional machining, and after that, the responses such as temperature, cutting force, residual stress and surface morphologies can be investigated and modeled using different evolutionary optimization techniques. The research of Al-li alloy machining and production will further meet the needs in aerospace industry.

Funding Statement: This research is supported by the National Natural Science Foundation of China (Grant Nos. 51475087 and 51304105), the Natural Science Foundation of Liaoning Province (Grant No. 20180550167), the Key Projects of Liaoning Province (Grant Nos. LJ2019ZL005 and LJ2017ZL001), and the Oversea Training Project of High Level Innovation Team of Liaoning Province (Grant No. 2018LNGXGJWPY-ZD001).

Conflicts of Interest: The authors declare that they have no conflicts of interest to report regarding the present study.

References

1. Yu, H. S., Zhan, X. H., Kang, Y., Xia, P. Y., Feng, X. S. (2018). Numerical simulation optimization for laser welding parameter of 5A90 Al-Li alloy and its experiment verification. *Journal of Adhesion Science and Technology, 33(2),* 137–155. DOI 10.1080/01694243.2018.1516503.
2. Chu, Q., Li, W. Y., Yang, X. W., Shen, J. J., Vairis, A. et al. (2018). Microstructure and mechanical optimization of probeless friction stir spot welded joint of an Al-Li alloy. *Journal of Materials Science & Technology, 34(10),* 1739–1746. DOI 10.1016/j.jmst.2018.03.009.
3. Muthumanickam, A., Gandham, P., Dhenuvakonda, S. (2019). Effect of friction stir welding parameters on mechanical properties and microstructure of AA2195 Al–Li alloy welds. *Transactions of the Indian Institute of Metals, 72(6),* 1557–1561. DOI 10.1007/s12666-019-01570-x.
4. Nayan, N., Gurao, N. P., Narayana Murty, S. V. S., Jha, A. K., Pant, B. et al. (2015). Microstructure and micro-texture evolution during large strain deformation of an aluminium–copper–lithium alloy AA 2195. *Materials & Design, 65,* 862–868. DOI 10.1016/j.matdes.2014.09.037.
5. Gairola, S., Joshi, A., Gangil, B., Rawat, P., Verma, R. (2019). Correlation of tensile properties and fracture toughness with microstructural features for Al–Li 8090 alloy processed by cryorolling and post-rolled annealing. *Transactions of the Indian Institute of Metals, 72(7),* 1743–1755. DOI 10.1007/s12666-019-01641-z.
6. Chen, Q. H., Lin, S. B., Yang, C. L., Fan, C. L. (2016): Effect of ultrasonic impact on the microstructure of welded joint of 2195 Al–Li alloy. *Acta Metallurgica Sinica (English Letters), 29(4),* 367–372. DOI 10.1007/s40195-016-0396-z.
7. Zhang, J., Feng, X. S., Gao, J. S., Huang, H., Ma, Z. Q. et al. (2018). Effects of welding parameters and post-heat treatment on mechanical properties of friction stir welded AA2195-T8 Al-Li alloy. *Journal of Materials Science & Technology, 34(1),* 219–227. DOI 10.1016/j.jmst.2017.11.033.

8. Wang, X. H., Wang, J. H., Yue, X., Gao, Y. (2015). Effect of aging treatment on the exfoliation corrosion and stress corrosion cracking behaviors of 2195 Al–Li alloy. *Materials & Design, 67,* 596–605. DOI 10.1016/j.matdes.2014.11.007.
9. Huang, J. L., Li, J. F., Liu, D. Y., Zhang, R. F., Chen, Y. L. et al. (2018). Correlation of intergranular corrosion behaviour with microstructure in Al-Cu-Li alloy. *Corrosion Science, 139,* 215–226. DOI 10.1016/j.corsci.2018.05.011.
10. Mou, H. K., Huang, X. D., Yuan, Y. C., Zhang, X. M., Ding, H. (2014). Investigation of surface integrity of Al lithium alloy in high speed machining (in Chinese). *Scientia Sinica Technologica, 44(1),* 89–98. DOI 10.1360/092013-1261.
11. Sahoo, P., Pratap, A., Bandyopadhyay, A. (2017). Modeling and optimization of surface roughness and tool vibration in CNC turning of Aluminium alloy using hybrid RSM-WPCA methodology. *International Journal of Industrial Engineering Computations, 8(3),* 385–398. DOI 10.5267/j.ijiec.2016.11.003.
12. Yahya, E., Ding, G. F., Qin, S. F. (2014). Sensitivity analysis and optimization of machining parameters based on surface roughness prediction for AA6061. *Applied Mechanics and Materials, 598,* 181–188. DOI 10.4028/www.scientific.net/AMM.598.181.
13. Hussain, M. A., Prasad, K. K., Jadhav, A. S., Biradat, G. (2017). Parametric optimization of CNC end milling process on aluminium 6063 alloy using grey based Taguchi method. *Applied Mechanics and Materials, 867,* 148–156. DOI 10.4028/www.scientific.net/AMM.867.148.
14. Liu, N., Wang, S. B., Zhang, Y. F., Lu, W. F. (2016). A novel approach to predicting surface roughness based on specific cutting energy consumption when slot milling Al-7075. *International Journal of Mechanical Sciences, 118,* 13–20. DOI 10.1016/j.ijmecsci.2016.09.002.
15. Zhang, H., Deng, Z. H., Fu, Y. H., Wan, L. L., Liu, W. (2017). Optimization of process parameters for minimum energy consumption based on cutting specific energy consumption. *Journal of Cleaner Production, 166(10),* 1407–1414. DOI 10.1016/j.jclepro.2017.08.020.
16. Carmita, C. N. (2014). Optimization of cutting parameters using response surface method for minimizing energy consumption and maximizing cutting quality in turning of AISI 6061 T6 aluminum. *Journal of Cleaner Production, 91(3),* 109–117. DOI 10.1016/j.jclepro.2014.12.017.
17. Rashmi, L. M., Karthik, M. C., Arun, K. S. (2016). Application of particle swarm optimization and response surface methodology for machining parameters optimization of aluminium matrix composites in milling operation. *Journal of the Brazilian Society of Mechanical Sciences and Engineering, 39(9),* 3541–3553. DOI 10.1007/s40430-016-0675-7.
18. Rashmi, L. M., Karthik, M. C., Arun, K. S., Shrikantha, S. R., Mervin, A. H. (2018). Machining parameters optimization of AA6061 using response surface methodology and particle swarm optimization. *International Journal of Precision Engineering and Manufacturing, 19(5),* 695–704. DOI 10.1007/s12541-018-0083-2.
19. Singh, G., Gupta, M. K., Mia, M., Sharma, V. S. (2018). Modeling and optimization of tool wear in MQL-assisted milling of Inconel 718 superalloy using evolutionary techniques. *International Journal of Advanced Manufacturing Technology, 97(1–4),* 481–494. DOI 10.1007/s00170-018-1911-3.
20. Gupta, M. K., Mia, M., Pruncu, C. I., Kaplonek, W., Nadolny, K. et al. (2019). Parametric optimization and process capability analysis for machining of nickel-based superalloy. *International Journal of Advanced Manufacturing Technology, 102(9–12),* 3995–4009. DOI 10.1007/s00170-019-03453-3.
21. Li, C. B., Xiao, Q. G., Tang, Y., Li, L. (2016). A method integrating Taguchi, RSM and MOPSO to CNC machining parameters optimization for energy saving. *Journal of Cleaner Production, 135(11),* 263–275. DOI 10.1016/j.jclepro.2016.06.097.
22. Jang, D. Y., Jung, J. Y., Seok, J. W. (2016). Modeling and parameter optimization for cutting energy reduction in MQL milling process. *International Journal of Precision Engineering and Manufacturing-Green Technology, 3 (1),* 5–12. DOI 10.1007/s40684-016-0001-y.
23. Zhou, J. H., Ren, J. X., Yao, C. F. (2017). Multi-objective optimization of multi-axis ball-end milling Inconel 718 via grey relational analysis coupled with RBF neural network and PSO algorithm. *Measurement, 102,* 271–285. DOI 10.1016/j.measurement.2017.01.057.

24. Chetan, Ghosh, S., Rao, P. V. (2018). Specific cutting energy modeling for turning nickel-based Nimonic 90 alloy under MQL condition. *International Journal of Mechanical Sciences, 146–147(10),* 25–38. DOI 10.1016/j.ijmecsci.2018.07.033.

25. Sarwar, M., Persson, M., Hellbergh, H., Haider, J. (2009). Measurement of specific cutting energy for evaluating the efficiency of bandsawing different workpiece materials. *International Journal of Machine Tools and Manufacture, 49(12–13),* 958–965. DOI 10.1016/j.ijmachtools.2009.06.008.

26. Velchev, S., Kolev, I., Ivanov, K., Gechevski, S. (2014). Empirical models for specific energy consumption and optimization of cutting parameters for minimizing energy consumption during turning. *Journal of Cleaner Production, 80,* 139–149. DOI 10.1016/j.jclepro.2014.05.099.

27. Albertelli, P., Keshari, A., Matta, A. (2016). Energy oriented multi cutting parameter optimization in face milling. *Journal of Cleaner Production, 137(11),* 1602–1618. DOI 10.1016/j.jclepro.2016.04.012.

28. Ghosh, G., Mandal, P., Mondal, S. C. (2017). Modeling and optimization of surface roughness in keyway milling using ANN, genetic algorithm, and particle swarm optimization. *International Journal of Advanced Manufacturing Technology, 100(5),* 1223–1242. DOI 10.1007/s00170-017-1417-4.

29. Nieto, P. J., Gonzalo, E., Vilán, J. A., Robleda, A. S. (2015). A new predictive model based on the PSO-optimized support vector machine approach for predicting the milling tool wear from milling runs experimental data. *International Journal of Advanced Manufacturing Technology, 86(1–4),* 769–780. DOI 10.1007/s00170-015-8148-1.

30. Sen, B., Hussain, S. A., Mia, M., Mandal, U. K., Mondal, S. P. (2019). Selection of an ideal MQL-assisted milling condition: an NSGA-II-coupled TOPSIS approach for improving machinability of Inconel 690. *International Journal of Advanced Manufacturing Technology, 103(5–8),* 1811–1829. DOI 10.1007/s00170-019-03620-6.

31. Meng, Y., Wang, L. H., Lee, C. H., Ji, W., Liu, X. L. (2018). Plastic deformation-based energy consumption modelling for machining. *International Journal of Advanced Manufacturing Technology, 96(1–4),* 631–641. DOI 10.1007/s00170-017-1521-5.